Quarterly Technical Report

Defects and Impurities in 4H- and 6H-SiC Homoepitaxial Layers: Identification, Origin, Effect on Properties of Ohmic Contacts and Insulating Layers and Reduction

Supported under Grant #N00014-95-1-1080
Office of the Chief of Naval Research
Report for the period 7/1/96-9/30/96

R. F. Davis, M. O. Aboelfotoh, B. J. Baliga*, R. J. Nemanich†,
S. W. King, L. S. Porter, S. Sridevan*, and H. S. Tomozawa
Department of Materials Science and Engineering
*Department of Electrical and Computer Engineering
†Department of Physics
North Carolina State University
Campus Box 7907
Raleigh, NC 27695-7907

September, 1996

REPORT DOCUMENTATION PAGE

Form Approved
OMB No. 0704-0188

1. AGENCY USE ONLY *(Leave blank)*	2. REPORT DATE	3. REPORT TYPE AND DATES COVERED
	September, 1996	Quarterly Technical 7/1/96–9/30/96

4. TITLE AND SUBTITLE
Defects and Impurities in 4H- and 6H-SiC Homoepitaxial Layers: Identification, Origin, Effect on Properties of Ohmic Contacts and Insulating Layers and Reduction

5. FUNDING NUMBERS
ydl495l---01
312
N00179
N66020
4B855

6. AUTHOR(S)
R. F. Davis, M. O. Aboelfotoh, B. J. Baliga and R. J. Nemanich

7. PERFORMING ORGANIZATION NAME(S) AND ADDRESS(ES)
North Carolina State University
Hillsborough Street
Raleigh, NC 27695

8. PERFORMING ORGANIZATION REPORT NUMBER
N00014-95-1-1080

9. SPONSORING/MONITORING AGENCY NAMES(S) AND ADDRESS(ES)
Sponsoring: ONR, Code 312, 800 N. Quincy, Arlington, VA 22217-5660
Monitoring: Administrative Contracting Officer, Regional Office Atlanta
Regional Office Atlanta, 101 Marietta Tower, Suite 2805
101 Marietta Street
Atlanta, GA 30323-0008

10. SPONSORING/MONITORING AGENCY REPORT NUMBER

11. SUPPLEMENTARY NOTES

12a. DISTRIBUTION/AVAILABILITY STATEMENT
Approved for Public Release; Distribution Unlimited

12b. DISTRIBUTION CODE

13. ABSTRACT *(Maximum 200 words)*

A SiC CVD system has been assembled to grow and dope 4H- and 6H-SiC thin films. The design incorporates a separate load lock from which the growth chamber and a RHEED chamber are attached. Power supply components remain to be received. Comparisons between the wetting characteristics of the on- and off-axis as well as the oxidized and unoxidized 6H-SiC$(0001)_{Si}$ surfaces in various acids and bases were made to that of Si(111). Both on- and off- axis oxidized 6H surfaces were hydrophilic after removal of the oxide with 10:1 HF and rinsing in DI water. In contrast, it was observed that both on and off axis as received/ as polished $(0001)_{Si}$ 6H-SiC surfaces were hydrophobic before and after dipping in 10:1 HF. Wet chemical cleans, specifically, RCA SC1 (1:1:5 $NH_3OH:H_2O_2:H_2O$) and Piranha Etch (7:3 $H_2SO_4:H_2O_2$) converted these hydrophobic surfaces into hydrophilic surfaces. The use of 200 Å of Si as a hydrophobic passivating layer has also been demonstrated. As-deposited NiAl, Au, Ni, and Pt contacts were rectifying on p-type 6H-SiC with very low leakage current densities ($\sim 1\times10^{-8}$ A/cm^2 at 10 V) and displayed a similar Schottky barrier trend as previously found for n-typeH-SiC. Ni/NiAl contacts on p-type (1×10^{19} cm^{-3}) SiC were ohmic after annealing for 10-80 s at 1000 °C with a specific contact resistivity of $2\text{-}3\times10^{-2}$ Ω•cm^2. Cr-B contacts were semi-ohmic on p-type SiC (1×10^{18} cm^{-3}) after annealing at 1000°C for 60-240 s in Ar, but became rectifying after annealing for 300 s, a result which may be due to the formation of B_4C. Oxidation of the Cr-B contacts was not observed. A mask set and associated MOS capacitors and MOS gated diodes on 4H- and 6H-SiC(0001) were designed and fabricated to characterize the SiO_2/SiC interfaces. An effective charge density of $\approx 2.2\times10^{12}$ cm^{-2} and an average interface trap density of 6.4×10^{11} cm^{-2}•eV^{-1} were measured from C-V measurements.

14. SUBJECT TERMS
chemical vapor deposition, 4H-SiC, 6H-SiC, silicon carbide, thin films, ohmic contacts, Schottky barrier height, NiAl, Au, Pt, Ni, hydrophobic, hydrophillic, contact restivity, MOS capacitor, MOS gated diode

15. NUMBER OF PAGES
33

16. PRICE CODE

17. SECURITY CLASSIFICATION OF REPORT	18. SECURITY CLASSIFICATION OF THIS PAGE	19. SECURITY CLASSIFICATION OF ABSTRACT	20. LIMITATION OF ABSTRACT
UNCLAS	UNCLAS	UNCLAS	SAR

Table of Contents

I. Introduction

The two most important materials-related problems affecting the performance of all SiC devices and their associated components (e.g., contacts) are the defects and the undesired impurities which become incorporated in the homoepitaxial SiC layers in which all devices are currently fabricated. Bhatnagar [1] has shown that the reverse blocking leakage current in high voltage Schottky diodes is three orders of magnitude higher than theoretically predicted as a result of defects in the epi-layer. The formation of micropipes, stepped screw dislocations, interacting dislocation loops, polyganized networks of dislocations and growth twins as well as stacking faults during the sublimation growth of SiC boules are likely the root cause of some of the defects in the epitaxial layer. However, with the exception of the micropipes, the types and concentrations of line, planar and other three-dimensional defects and their effect on the performance of devices and individual device components in the important epi-layer have not been similarly determined. As such, it is not known which of the latter defects actually are translated from the wafer into the epi-layer during its deposition and, therefore, should be vigorously controlled during boule growth and which defects are generated during deposition.

The relatively uncontrolled occurrence of the n-type donor of N and deep level compensating impurities such as Ti in the epilayer have been identified via secondary ion mass spectrometry, photoluminescence and cathodoluminescence investigations. However, the origins of essentially all of these impurities are unknown. For high-temperature, -power and -frequency devices, it is highly desirable to control or eliminate these impurities such as to attain undoped films with uncompensated carrier concentrations of 10^{14} cm^{-3}—two orders of magnitude lower than what is, at present, normally achieved in standard commercial depositions.

The formation of low resistivity and thermally stable ohmic contacts to 4H- and 6H-SiC remains a serious problem in the development of SiC device technology. For SiC power devices to have an advantage over Si, the contact resistivities must be below 1×10^{-5} W-cm^2, as noted by Alok, *et al.* [2]. In addition, the electrical characterization of state-of-the-art SiC films depends on the ability to fabricate ohmic contacts on material with low carrier concentrations. Therefore, better ohmic contacts are needed both for improving device performance and for improving the quality of films which can be grown. The thermal stability of ohmic contacts is of particular concern for p-type SiC, which have traditionally relied on low melting point Al or Al alloys to dope the SiC surface below the contacts. These materials are not suitable for devices intended for high-temperature operation. While the fabrication of ohmic contacts to SiC has also normally depended on the attainment of a very heavily-doped near-surface region, the introduction during deposition of high levels of dopants in the near surface device region of the epi-layer prior to the deposition of the contact or by ion implantation through the contact makes probable the introduction of point and line defects as a result of the induced strain in the lattice.

Based on all of these issues and recent experiments already performed at NCSU, our goals are to produce contacts which are thermally stable and have low contact resistivities while also reducing the need for doping by ion implantation.

To fabricate most microelectronic devices, the growth or deposition of stable insulators is needed to provide both passivating layers and gate dielectrics. Silicon carbide is almost invariably thermally oxidized, albeit at a slower rate, in the same manner and temperature range that is employed for Si. Most of the previous studies regarding the oxidation of SiC have been concerned with polycrystalline materials. It has been shown by Harris and Call [3] and Suzuki, *et al.* [4] that the (0001) face of 6H-SiC oxidizes according to the same linear-parabolic equation reported for Si by Deal and Grove [5]. The model states that the initial stage of oxidation is reaction rate limited and linear, but becomes parabolic as the diffusion of the oxidant through the oxide becomes the rate limiting factor. Research at NCSU by Palmour *et al.* [6] has demonstrated that the oxidation process on SiC in wet and dry oxygen and wet argon obeys the linear-parabolic law. Both wet processes had a slower rate than dry oxidation at 1050°C and below. The dry oxides exhibited a very flat surface; in contrast, SEM and TEM revealed that wet oxidation preferentially oxidizes dislocation bands, causing raised lines on the oxide and corresponding grooves in the SiC. It was proposed that the much higher solubility of H_2O in SiO_2 as compared to that of O_2 allows wet oxidation to be preferential.

All of the oxidation studies on all polytypes of semiconductor quality SiC have been conducted on n-type material with the exception of the investigation by Palmour *et al.* [6]. The objective of this study was the determination of the redistribution of the common electrical dopants of N, P, Al and B during thermal oxidation of SiC films at 1200°C in dry O_2. Experimental segregation coefficients and interfacial concentration ratios were determined. Secondary ion mass spectrometry revealed that B and Al depleted from the SiC into the growing oxide while N and P were found to pile up in the SiC as a result of the loss of the SiC to the oxide formation. Aluminum is now used almost universally as the p-type dopant in SiC. The electrical properties of oxides thermally grown on n-type SiC normally have reasonably favorable characteristics of high breakdown voltage and low leakage currents. However, the reverse is true for thermally grown oxides on p-type SiC, as shown by Baliga and his students at NCSU. It is believed that at least two of the causes of the poor performance on a p-type material are the existence of the Al in the oxide and at the oxide/SiC interface and the dangling oxygen bonds which this species creates in the oxide as a result of a difference in oxidation state (+3) compared to that of Si (+4) and the existence of C at the SiC/insulator interface. Methods of effectively cleaning SiC surfaces prior to oxidation to deposit and grow oxides on p-type material under UHV conditions and determine the effect of Al redistribution and C concentrations at the interface on the properties of the oxide must be determined. In addition,

the effect of existing line and planar defects in the SiC epi-layer on the properties of the thermally grown and deposited oxide must be ascertained.

The research conducted in this reporting period and described in the following sections has been concerned with (1) design and construction of a new CVD SiC system for the deposition and doping of 6H- and 4H-SiC and AlN films, (2) studies of *ex situ* cleaning of the on- and off-axis as well as the oxidized and unoxidized 6H-SiC$(0001)_{Si}$ surfaces in various acids and bases, (3) deposition, annealing and electrical characterization of Ni, NiAl, Au, Pt and Cr-B contacts to p-type SiC(0001), and (4) fabrication of MOS capacitors and MOS gated diodes on 4H- and 6H-SiC(0001). The following individual sections detail the procedures, results, discussions of these results, conclusions and plans for future research. Each subsection is self-contained with its own figures, tables and references.

References

1. M. Bhatnagar, Ph. D. Thesis, North Carolina State University, 1994.
2. D. Alok, B. J. Baliga and P. K. McLarty, IEDM Technical Digest, IEDM 1993, 69 (1993).
3. R. C. A. Harris and R. L. Call in *Silicon Carbide–1973*, R. C. Marshall, J. W. Faust and C. E. Ryan, Eds. University of South Carolina Press, Columbia, S. C., 1974, p. 534.
4. Suzuki, *et al.*, Jap. Journ. Appl. Phys. **21**, 579 (1982).
5. B. E. Deal and A. S. Grove, J. Appl. Phys. **36**, 3770 (1965).
6. J. W. Palmour, R. F. Davis, H. S. Kong, S. F. Corcoran and D. P. Griffis, J. Electrochem. Soc. **136**, 502 (1989).

II. Design and Construction of Silicon Carbide Chemical Vapor Deposition System

A. Introduction

A system is being built in order to grow silicon carbide thin films of high quality. A design has been developed. Many parts have been received and have been assembled, and construction on the electrical and gas lines is currently underway.

B. Experimental Procedure

The system design is comprised of a six-way cross, serving as a loadlock, from which two separate chambers are attached. Off of this loadlock to one side is a growth chamber. To another side, perpendicular to the axis of the loadlock and growth chamber, is the sescond chamber where RHEED analysis will be performed. The sample will be transferred to and from the various chambers on a SiC-coated graphite susceptor platform upon which the sample will be placed. The transfer mechanism consists of a platform which is moved from chamber to chamber by means of a manipulator rod, which is screwed to the side of the susceptor.

The growth chamber consists of a rotating module, to which the susceptor is attached. Growth will occur on the sample in an upside-down position, with gases flowing upward, while the susceptor is being rotated. The susceptor is attached to the rotating rod assembly by a groove into which the susceptor slides when transfer of the sample takes place. Once the sample is transferred to the rotating rod, the rod is brought down to the quartz portion of the reaction chamber. Here, the sample is heated via RF coil and gases are introduced from the bottom of the reactor. Growth temperature will be monitored by means of a standing pyrometer mounted outside the quartz chamber, aimed at the sample. Growth processes, such as gas flow rate and pressure, will be monitored by electronic components. Gas flow will be controlled by mass flow controllers, and pressure by capacitance manometers.

The RHEED (reflection high-energy electron diffraction) chamber, attached on another side of the loadlock chamber, will be attached to monitor film crystallinity, crystal structure and the formation of new surfaces. Since growth of high-quality crystalline SiC films is being attempted, a RHEED chamber that is attached to a nominal high vacuum to prevent direct exposure to atmosphere after growth will be useful to characterize the film.

The SiC growth process will consist of introducing SiH_4 and C_2H_4 as the reactive components carried by a H_2 carrier. Nominal flow values will be on the order of 1 to 10 sccm for each. Carrier flows of H_2 will be on the order of 3 liters per minute. Other gases that will be included on the system will be NH_3 and an N_2/H_2 mixture, for doping, and Ar. TEA will also be used for doping, which will be kept at constant temperature by a heater bath.

C. Results

To date, the following has been accomplished: a design has been developed where sample transfer, growth, and RHEED analysis have been determined; a support frame to provide physical support to the system has been designed and built; three six-way crosses have been put together with the adjoining gate valves on the frame, and available flanges and window ports have been attached; a quartz chamber-to-cross assembly has been machined, which will provide a sealed interface between two parts of the growth chamber; quartz cylinders have been cut to design dimensions; flange parts, pressure gauge attachments, pump connection parts, and a rotating rod assembly, have been machined; an RF generator has been refurbished and returned to us to be used to provide RF heating to the susceptor; and assembly of a switch panel to control the nupro valves and to enable computer control.

Currently in progress are the following: a RHEED chamber manipulator is being fitted with a holder which will accommodate the susceptor upon transfer; electrical wiring of the switch panel to control the nupro valves is being assembled; assembly of the various gas lines on a panel to be mounted on one side of the system is being performed. Electrical and water facilitation of the system has been requested. This entails discussions with the NCSU Department of Environmental Health and Safety, the State of North Carolina Department of Insurance, and the NCSU Physical Plant Engineering and Design Departments, which must all agree on the layout of the facilities modification request.

D. Discussion

The proposed design was developed with many sources of input. A number of constraints determined the design configuration and materials used in the system. One of the main concerns was the high operating temperature of the growth chamber. Since temperatures around 1600-1700°C were going to be used to grow SiC thin films, it was determined that quartz would be the best material for the growth portion of the chamber. Once this was determined, a design had to be developed to cool the chamber. A double-walled quartz vessel, water cooled around the perimeter, was determined to be the optimum mode of cooling.

Another concern was the transfer mechanism of the susceptor and the placement of samples on the susceptor surface. It was decided that small silicon carbide screws would be the most flexible for our purposes to accommodate various-sized samples. For the transfer mechanism, a simple tongue-in-groove assembly, moved between chambers by means of a transfer arm which would screw into the side of the susceptor, was deemed simplest and most practical.

E. Future Research Plans and Goals

Most components have been designed, received or are currently being machined. Further assembly of the system is expected when facilitation of electrical and water inputs to the building enable testing of parts of the system.

III. Wet Chemical Processing of $(0001)_{Si}$ 6H-SiC: Hydrophobic and Hydrophilic Surfaces

A. Introduction

For SiC to succeed as the substrate/semiconductor of choice for high-frequency/high-temperature, high-power devices and III-N heteroepitaxy, a considerable reduction in defects (line, planar, point, etc.) must be achieved. Following Si technology, where surface cleaning and preparation are critical first steps in all processes [1], a continued reduction in defects in SiC should be expected as a result of improved SiC wafer surface cleaning/preparation techniques. In Si technology, for example, improper removal of surface contamination and oxides prior to Si homoepitaxy has been shown to result in an increase in the density of line and planar defects in epitaxial films from $< 10^4/cm^2$ to $> 10^{10}/cm^2$ [2-4] and an associated drop in device yield [5]. In the case of heteroepitaxy, studies on Si_xGe_{1-x} alloy growth on Si (100) have additionally shown that surface defects produced in the Si substrate by residual organic/carbon contamination act as the preferred sites for misfit dislocation generation [6]. This clearly illustrates that surface preparation should be equally important to the control of defects in both homoepitaxial and heteroepitaxial growth of SiC and III-V nitrides on 6H-SiC.

As a limited number of studies have been conducted on *ex situ* SiC cleaning practices [7-10], most SiC *ex situ* wet chemical processing is still based on processes developed specifically for and employed in Si microelectronics technology [10,11]. Thus stated, typical SiC *ex situ* cleaning/surface preparation consists of some variation of solvent degreasing, organic contaminant removal using an RCA clean or Piranha etch, and finishing with oxide removal in an HF based solution [7-11]. In Si technology, oxide removal with HF as a last step has been popular due to the fact that it generates a hydrophobic, hydrogen terminated surface, stable against oxidation in air for several hours [12-17]. The hydrogen termination further prevents reaction of the bare Si wafer with organic contaminants to form Si-C crystallites which have been shown to generate a variety of structural and electrical defects [1]. The hydrophobic surface can also assist in reduction of particulates as the wafer is drawn across a liquid/air interface which is known to harbor a variety of microparticulates and organic contaminants [1,5].

For the case of SiC, it has not yet been established and/or demonstrated that HF wet chemical processing produces a hydrogen terminated/hydrophobic surface. This report directly compares to Si (111) the wetting characteristics of $(0001)_{Si}$, $(000\text{-}1)_C$, (11-20), and (10-10) 6H-SiC surfaces after an HF dip. The results show clearly that regardless of orientation, 6H-SiC surfaces are inherently hydrophilic with respect to Si. With this in mind, attempts to identify and demonstrate other passivating layers which yield hydrophobic SiC surfaces will be made.

B. Experimental Procedure

On-axis and vicinal n-type (typically $N_d=10^{18}/cm^3$) $(0001)_{Si}$ 6H-SiC wafers were used in these experiments. These wafers were by supplied Cree Research, Inc. with and without a 500-1000Å thermally grown oxide. Both the oxidized and "as polished" (i.e. not oxidized) 6H-SiC wafers were ultrasonically cleaned/degreased in tricholorethylene, acetone, and methanol each for 10 min. prior to any other wet chemical treatments. The oxide was removed from the thermally-oxidized wafers using a 10 min. dip in a 10:1 HF solution, followed by rinsing in de-ionized (DI) water and N_2 blow drying. The wetting characteristics of this surface and the unoxidized surfaces were then investigated by immersion in other acid/base solutions. The wet chemistries examined included 10:1 HF, 10:1 buffered HF (7:1 NH_4F:HF), 30:1 buffered HF, 40% NH_4F, 38% HCl, 70% HNO_3, Pirahna Etch (7:3 H_2SO_4:H_2O_2), RCA SC1 & SC2 (1:1:5 NH_3OH:H_2O_2:H_2O and 1:1:5 HCl:H_2O_2:H_2O@85°C), $HC_2H_3O_2$, and 40% KOH. Except where noted, after all wet chemical treatments the samples were rinsed in DI water (18M) and blown dry with N_2. At this point it was visually determined whether a hydrophobic or hydrophilic surface had been obtained. All wet chemicals were of CMOS grade purity (J.T. Baker)

Surfaces prepared in the above manner were further subjected to surface analysis in an integrated ultra-high vacuum system incorporating the following analytical techniques: X-ray Photoelectron Spectroscopy (XPS), Auger Electron Spectroscopy (AES), Electron Energy Loss Spectroscopy (EELS), and Low Energy Electron Diffraction (LEED). Details of this system are given elsewhere [8]. After each wet chemical treatment above, the SiC wafer was mounted to a molybdenum sample holder and loaded into a load lock for subsequent analysis by AES, XPS, EELS, and LEED. XPS analysis was performed using the Al anode (hv=1486.6 eV) at 20mA and 12 kV. AES spectra were obtained using a beam voltage of 3 keV and an emission current of 1 mA. EELS spectra were obtained using a 100 eV electron beam and an emission current of 1 mA. LEED was performed using rear view optics, a beam voltage of approximately 115 eV, and an emission current of 1 mA. Calibration of the XPS binding energy scale was performed by measuring the position of the Au $4f_{7/2}$ and shifting the spectra such that the peak position occurred at 83.98 eV.

C. Results

$(0001)_{Si}$ 6H-SiC, Oxidized. Figure 1(a) displays an AES survey spectrum taken from an off axis $(0001)_{Si}$ 6H-SiC wafer after removal of the 750Å thermal oxide with a 10 min. 10:1 HF dip (Note: similar results were obtained as well for on axis, $(0001)_{Si}$ 6H-SiC). Si, C, and significant amounts of oxygen were detected. Unlike Si (111), the 10:1 HF solution was observed to wet the surface as it was slowly withdrawn from the HF solution (the HF solution did, however, slowly pool up on the surface). After rinsing in DI water, the surface was

observed to be clearly wetted by the H_2O (i.e. no pooling up of the H_2O). XPS analysis of this surface with and without a DI rinse after the HF dip revealed the presence of significantly higher amounts of fluorine on the surface not rinsed in DI vs. the DI rinsed sample (see Fig. 2a). In fact, fluorine was not detected by XPS for HF dipped surfaces rigorously rinsed in DI (see Fig. 2b). In general, the levels of fluorine coverage were observed to vary from day to day. Most importantly, the fluorine surface coverage was found to be somewhat dependent on the micropipe density in the SiC wafer. Wafers with high micropipe densities were found to outgas vigorously in vacuum, presumably due to HF trapped in the micropipes.

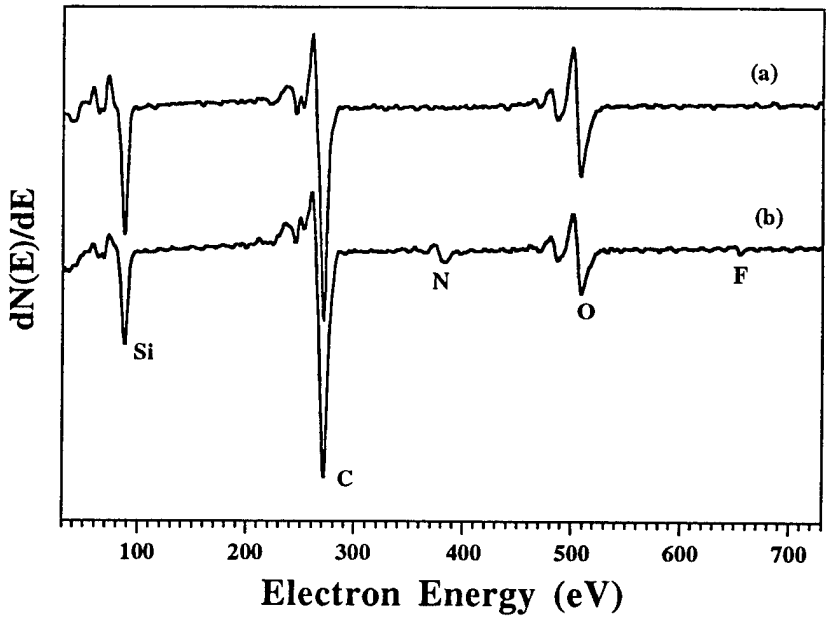

Figure 1. AES spectrum of (0001)Si 6H-SiC, off axis wafer (a) oxidized and dipped in 10:1 HF for 10 min., (b) no oxide and after solvent cleaning.

In agreement with the observed hydrophilic nature of these surfaces, the $(0001)_{Si}$ 6H-SiC surfaces after an HF dip were found to exhibit a much larger surface coverage of oxygen (approaching 1/2-3/4 monolayer) in comparison to Si (111) or Si (100) (see Fig. 3). The surface coverage of oxygen was not found to change appreciably with dipping time, HF concentration, composition, or pH. In addition to the increased surface coverage of oxygen, the presence of significant amounts of non-carbidic carbon were also detected by XPS. Figure 4(a), shows an XPS spectrum of the C 1s core level taken from a $(0001)_{Si}$ 6H-SiC surface after an HF dip. As can be seen, two C 1s peaks are detected with the lower binding energy peak at 282.8 eV corresponding to C-Si bonds and the higher binding energy peak located at 284.7 eV most likely corresponding to C-O, C=O, and O-C=O bonding (XPS results from this surface are summarized in Tables I and II). In contrast, EELS did not detect the presence of

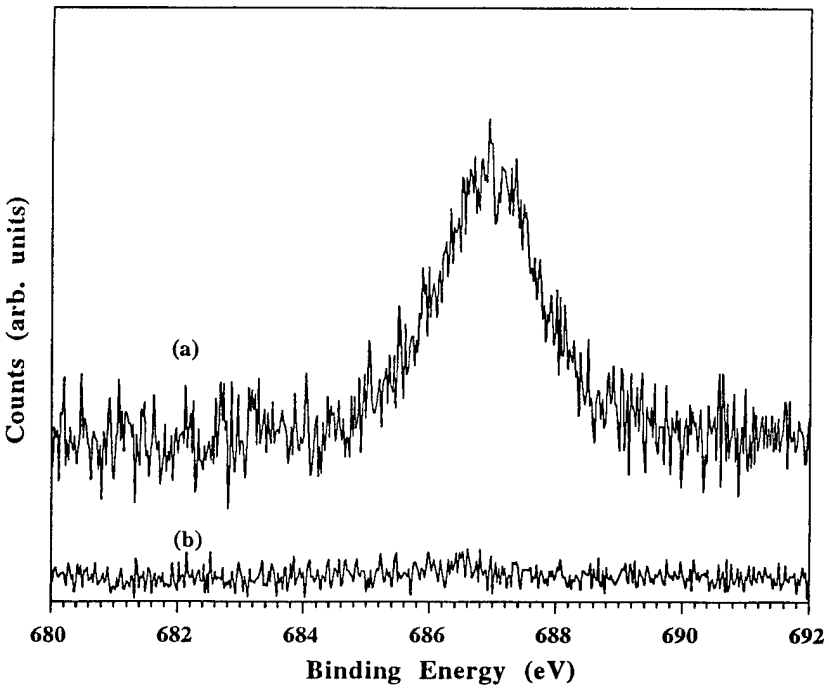

Figure 2. Oxidized (0001)Si 6H-SiC wafer after: (a) a 10 min. dip in 10:1 HF and blown dry without a DI rinse, (b) a 10 min. dip in 10:1 HF and rigorously rinsed in DI water.

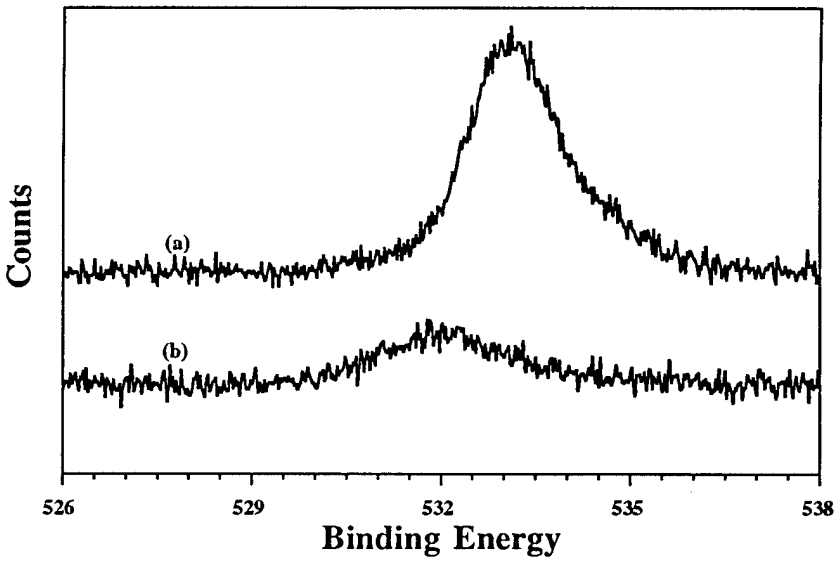

Figure 3. XPS spectrum of O 1s from (a) $(0001)_{Si}$ 6H-SiC and (b) (111)Si after a 10:1 HF dip.

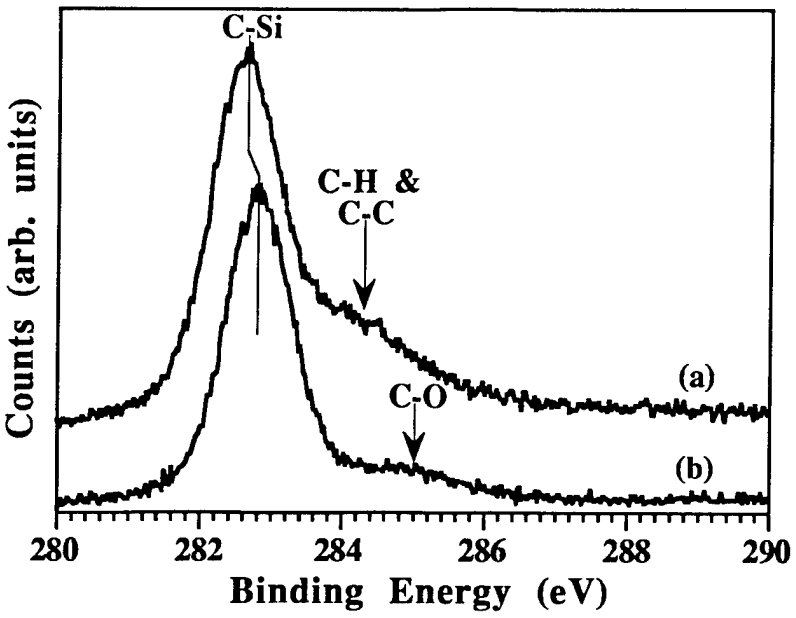

Figure 4. XPS spectrum of C 1s from (a) unoxidized $(0001)_{Si}$ 6H-SiC, and (b) oxidized $(0001)_{Si}$ 6H-SiC after a 10:1 HF dip.

Table I. Core Level Positions from $(0001)_{Si}$ 6H-SiC as Polished and Oxidized Surfaces after Various Treatments

Treatment	Si 2p, FWHM	O1s	C1s	F1s	N1s
As polished					
Solvents	100.5, 1.4 eV	531.9, 2.3 eV	282.6, 1.1 eV	685.8, 1.9 eV	398.2, 3.0 eV
			283.9, 2.7 eV	687.5, 2.5 eV	
10:1 HF	100.5, 1.4	531.6, 2.4	282.5, 1.1 eV	686.6, 1.9 eV	398.2, 3.0 eV
			283.6, 2.7 eV	687.3, 2.5 eV	
			285.8, 4.4 eV		
H_2SO_4:H_2O_2	100.4, 1.4	531.5, 2.5	283.5, 1.1	686.0, 3.0 eV	398.2, 3.0
			283.6, 2.7		
RCA SC1	100.3, 1.4	531.3, 2.8	282.4, 1.1		
			283.9, 2.4		
Aqua Regia	100.5, 1.4	531.6, 2.3	282.6, 1.1	685.5, 1.7	398.2, 3.0
			283.7, 2.7	686.9, 3.2	
Oxidized					
10:1 HF	100.7, 1.4	532.1, 1.9	282.8, 1.1		
			284.7, 2.1		

Table II. Summary of XPS Si/O, Si/F, C/C, and C-C Data

Treatment	Si/O	Si/F	C/C	C-C
As Polished				
Solvents	1.2	1.6	1.1	1.3 eV
10:1 HF	1.8	1.8	0.9	1.1 eV
H_2SO_4:H_2O_2	0.9	4.0	1.1	1.1 eV
RCA SC1	1.0	∞	2.2	1.5 eV
Aqua Regia	1.2	3.8	1.2	1.1 eV
Oxidized				
10:1 HF	1.4	∞	6.65	1.9 eV

transitions typically observed from organic molecules/contamination (see Fig. 5a). As mentioned by Mizokawa *et al.* [9], the failure of EELS to detect non-carbidic carbon could be due to electron stimulated desorption. Due to the inherent asymmetry of the Si 2p arising from an unresolved Si $2p_{3/2,1/2}$ doublet, it was impossible to accurately determine if a Si-O bonding peak existed. (1×1) LEED patterns with fuzzy dots were clearly displayed by these surfaces at E_p as low as 100 eV.

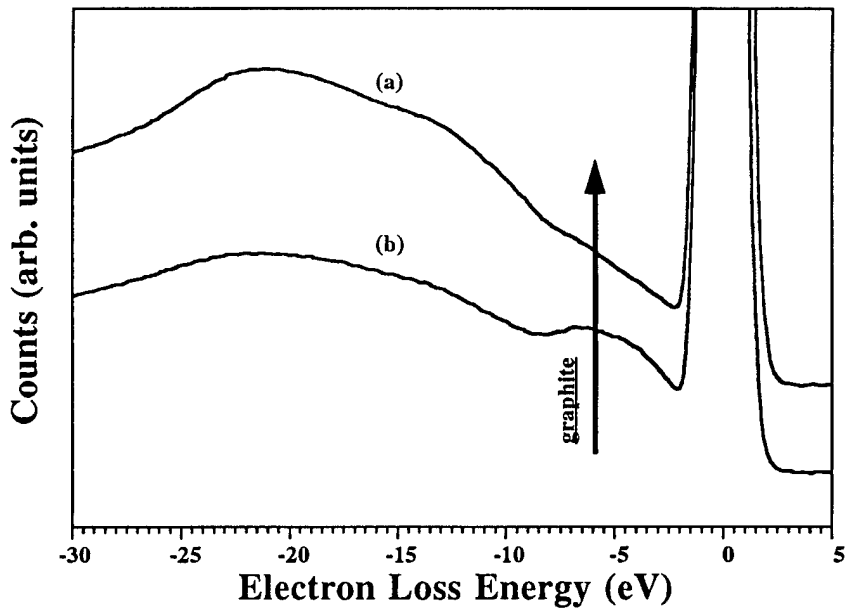

Figure 5. EELS of $(0001)_{Si}$ 6H-SiC (a) oxidized and a 10:1 HF dip, (b) unoxidized and solvent cleaned.

Following the 10:1 HF dip, the oxidized $(0001)_{Si}$ 6H-SiC surfaces were dipped in a variety of different acids and bases and the surface wetting characteristics visually noted. The results are summarized in Table III and illustrate that this surface was found to be hydrophilic in all acids and bases investigated.

Table III. Summary of Wetting Characteristics of as Polished and Oxidized $(0001)_{Si}$ 6H-SiC and (111) Si

Treatment	$(0001)_{Si}$ 6H-SiC As Polished	$(0001)_{Si}$ 6H-SiC Thermally Oxidized	(111) Si & Si Passivated 6H-SiC
10:1 HF	Hydrophobic	Hydrophilic	Hydrophobic
38% HCl	Phobic	Philic	Phobic
70% HNO_3	Phobic	Philic	Philic
RCA SC1	Philic	Philic	Philic
RCA SC2	Phobic	Philic	Philic
Piranha	Philic	Philic	Philic
Aqua Regia	Phobic	Philic	Philic
Acetic	Phobic	Philic	Phobic
NH_4F	Phobic	Philic	Phobic
KOH	Phobic	Philic	Philic

$(000\text{-}1)_C$, (11-20), and (10-10) 6H-SiC Surfaces. Thermally oxidized surfaces of other orientations of 6H-SiC such as $(000\text{-}1)_C$, (11-20), and (10-10) were also investigated. After removal of the oxide with 10:1 HF, these surfaces were also observed to be hydrophilic and very little differences were observed with the $(0001)_{Si}$ orientation. Figure 6 displays a series of AES spectrums taken from all four orientations investigated after removal of the thermal oxide with HF (note all spectra are normalized to the C KLL Auger transition). Table IV lists the Si/C, O/Si, and O/C pph ratios (uncorrected for differences in sensitivity) calculated for each surface. Table IV also shows the O/C ratio for all the different orientations of 6H-SiC surfaces to be centered around 0.3. Given that two of these surfaces are polar and the others non polar, it is surpassing that they would exhibit this similarity. Further, the Si/C ratio for the $(0001)_{Si}$, (11-20), and (10-10) surfaces are all centered around 0.6 which is surpassing in that the ideally $(0001)_{Si}$ surface would be terminated exclusively with Si, whereas the (10-10) and (11-20) are nonpolar surfaces ideally with equal numbers of carbon and silicon atoms at the outermost surface. The $(000\text{-}1)_C$ surface, however, shows a Si/C ratio half that found for $(0001)_{Si}$ which

is expected based on the differences in polarity for these two surfaces. The O/Si ratio for the $(000\text{-}1)_C$ surface was found to be twice that for the other orientations indicating the possibility that a significant amount of oxygen is actually bonded to carbon at the SiC surfaces.

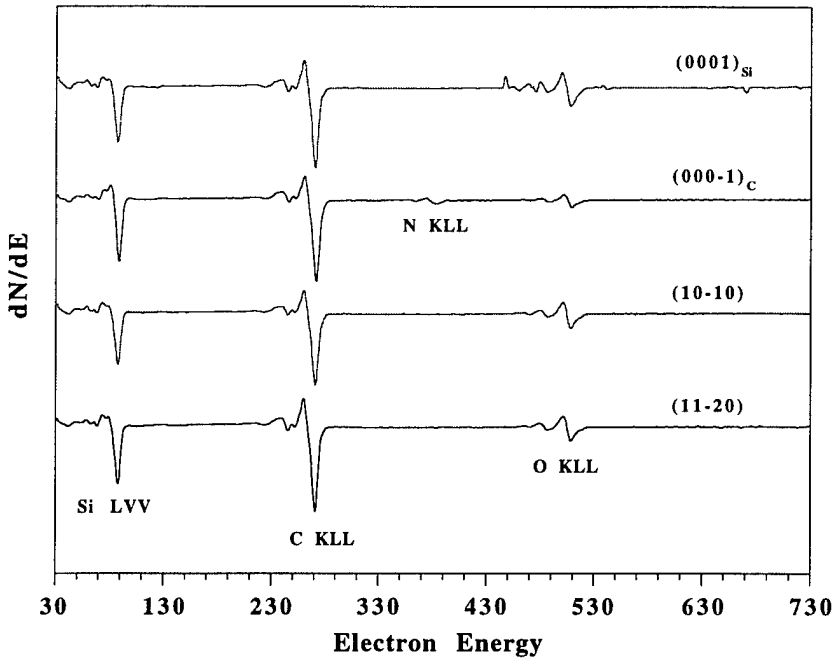

Figure 6. AES spectrums taken at various 6H-SiC surface orientations after removal of a thermal oxide with 10:1 HF.

Table 4. Peak to Peak Height (pph) Ratios for Various 6H-SiC Surfaces

	(0001)Si	(000-1)C	(11-20)	(10-10)
Si/C	0.60	0.34	0.61	0.65
O/Si	0.52	0.99	0.37	0.43
O/C	0.31	0.34	0.23	0.28

$0001)_{Si}$, No Oxide. As polished/unoxidized $(0001)_{Si}$ 6H-SiC on and off axis surfaces were observed to be hydrophobic as received without any further processing. Figure 1(b) displays an AES survey spectrum taken from an as polished off axis $(0001)_{Si}$ 6H-SiC surface after ultrasonic solvent cleaning and degreasing (tricloroethylene, acetone, and methanol; 10 min. each). In contrast to the hydrophilic oxidized SiC surfaces, traces of N and F were detected in addition to the presence of Si, C, and O, as shown in Fig. 1(b). The presence of F

was confirmed by XPS analysis as shown in Fig. 7(a). Further comparison of Figs. 1(a) and 1(b) reveals that the oxygen surface coverage for the solvent cleaned, as polished $(0001)_{Si}$ 6H-SiC surface is actually lower than the HF dipped oxidized SiC surface.

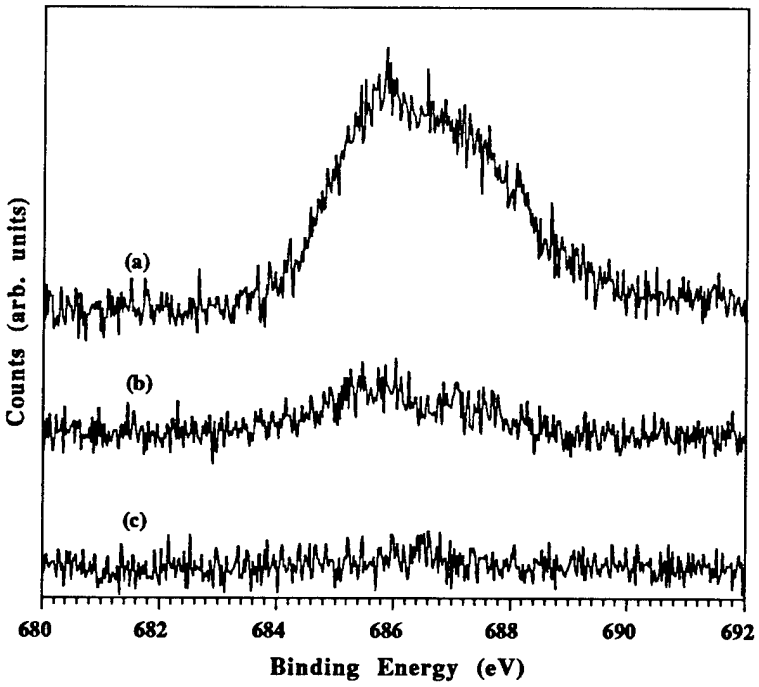

Figure 7. XPS of F1s from unoxidized/as polished $(0001)_{Si}$ 6H-SiC (a) after solvent cleaning, (b) 5 min. Piranha etch, (c) prolonged etching in RCA SC1.

Like the oxidized SiC surfaces, XPS analysis detected the presence of significant amounts of non-carbidic carbon on the solvent cleaned surface. Figure 4(b) shows an XPS spectrum of the C 1s core level taken from this surface. Two peaks are clearly detected: one at 282.6 eV indicative of Si-C bonding, and one at 283.9 eV indicative of C-C and C-H bonding. (See Table I for Si2p, O1s, C1s, N1s, and F1s core level positions). In addition, a detailed analysis of an on axis, as polished $(0001)_{Si}$ 6H-SiC surface revealed the presence of a third non-carbidic carbon peak at ≈ 285.8 eV (see Fig. 8a). A loss peak at 5-6 eV indicative of the -* transition of graphite like carbon was also detected in EELS (see Fig. 5a). A (1×1) diffraction pattern was barely discernible in LEED at E_p=100eV and only clearly discernible at $E_p \approx 180$ eV.

After dipping in 10:1 HF for 10 min., the as polished surface was still observed to be hydrophobic when rinsed in DI water. Non-carbidic carbon, F and N were also still detected by XPS, AES, and EELS. As shown in Fig. 9(a), the HF dip removed some oxygen from the surface. This was also seen in the XPS data where the Si2p/O1s ratio was found to increase after the HF dip (see Table II). However the C1s(Si-C)/C1s(C-C) ratio decreased indicating

that the HF dip left more non-carbidic carbon on the surface. Additionally, the non-carbidic C1s peak was observed to shift from 283.9 eV to 283.6 eV (see Table I). The amounts of F and N were not observed to change significantly with the HF dip.

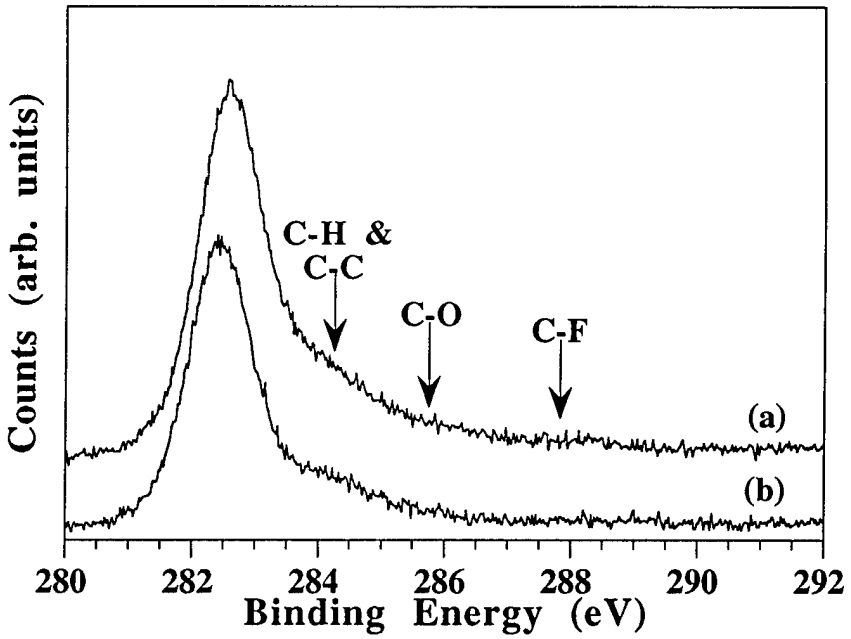

Figure 8. XPS of C 1s unoxidized/as polished (0001)Si 6H-SiC (a) after 10:1 HF dip, and (b) after extended etching in RCA SC1.

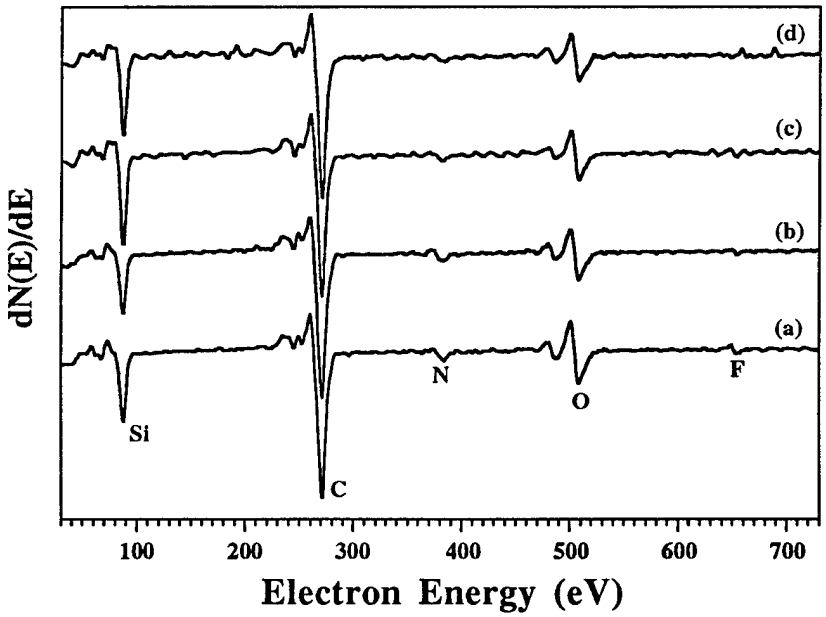

Figure 9. AES of $(0001)_{Si}$ 6H-SiC as polished after (a) solvent cleaning, (b) 10:1 HF dip, (c) 5 min. Pirahna Etch, and (d) 30 min. RCA SC1 clean.

After the 10:1 HF dip, the as polished SiC surface was observed to remain hydrophobic when dipped in various acids such as HCl and HNO_3, but would became hydrophilic in extended dip/etches in RCA SC1 or H_2SO_4:H_2O_2 (Piranha etch). In some cases, this hydrophilic surface could be made hydrophobic again by boiling in Aqua Regia (3:1 HCl:HNO_3) for 5-10 min. However, this was not always observed to be the case. Subsequent XPS analysis revealed complete removal of fluorine from hydrophobic $(0001)_{Si}$ 6H-SiC surfaces which had been permanently converted to hydrophilic surfaces by prolonged immersion in RCA SC1 (see Fig. 10a). In cases where hydrophilic $(0001)_{Si}$ 6H-SiC surfaces were observed to be converted back to hydrophobic surfaces by a boiling Aqua Regia treatment, XPS revealed incomplete removal of fluorine from the surface by the RCA SC1 or Piranha etch treatment (see Fig. 10b). In addition, the third C1s peak observed at 285.8 eV was observed to track with the fluorine coverage suggesting that this surface is terminated with fluorocarbons. A summary of the wetting characteristics observed for this surface after various wet chemical treatments is provided in Table III.

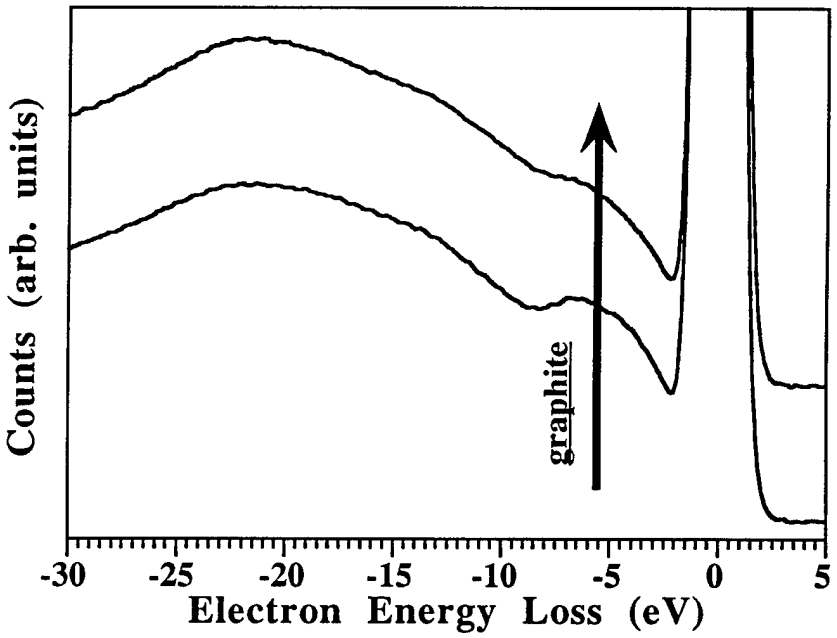

Figure 10. EELS of $(0001)_{Si}$ 6H-SiC after (a) 10:1 HF and (b) RCA SC1.

Si Passivating Layer. As there were no wet chemical treatments identified which could produce a hydrophobic surface from an oxidized $(0001)_{Si}$ 6H-SiC surface, a 200Å Si capping layer was investigated as an alternate hydrophobic passivating layer for this surface. The following procedure was used to prepare the capping layer. First, the $(0001)_{Si}$ 6H-SiC wafer was given a 10 min. dip in 10:1 HF, DI rinsed, N_2 blow dried, and loaded into a Si-Ge MBE

where it was then degassed and annealed at 1000°C for 20 min. in a 10^{-6} Torr SiH_4 flux. This produced an oxygen-free, Si-rich (1×1) SiC surface. Next, a Si e-beam was used to deposit 200Å of Si on the SiC surface at room temperature *in situ*. The Si/SiC sample was then removed from vacuum. The Si/SiC sample was dipped in 10:1 HF and observed to hydrophobic similar to Si (100) and (111) surfaces. The wetting characteristics of this surface in other acids and bases were additionally observed to be similar to those of silicon. This Si capping/passivating layer could be easily removed/desorbed *in situ* by annealing in vacuum at 1000-1100°C for 5-10 min. leaving behind a silicon rich, (3×3) reconstructed SiC surface.

D. Discussion

$(0001)_{Si}$ 6H-SiC, Oxidize. As the data presented above illustrates, copious amounts of oxygen and non-carbidic carbon are left unremoved from oxidized $(0001)_{Si}$ 6H-SiC after oxide removal using 10:1 HF. As essentially all *ex situ* cleaning practices are inherently imperfect due to the imperfect ambient in which they are conducted, the presence of small quantities of contaminants such as oxygen and carbon are to be expected. However, the amounts detected on $(0001)_{Si}$ 6H-SiC after removal of an oxide with HF are several times (3-4) larger than those detected on silicon in our laboratory under the same processing conditions. The observation of a hydrophilic surface as opposed to a hydrophobic surface illustrates that the chemistry and interactions occurring at Si and SiC surfaces in HF are clearly different.

The large levels of oxide left on the surface of SiC after an HF dip are particularly surprising given that concentrated HF is known to etch silicon oxide at rates as high as 50,000Å/sec [5]. Clearly something is prohibiting the HF from removing the last monolayer of oxide on the SiC surface. One possible explanation would be that the surface oxygen must be removed with the silicon atom to which it is attached. Due to the strong Si-C bond in comparison to the Si-Si bond, HF may not be able to break the Si-C back bond at the surface and, hence, remove the oxide. This would be in agreement with the fact that HF is known to not etch SiC. An alternative explanation, is that HF can break the Si-C bond and remove the Si-O, but does not remove the carbon from the surface. Over time, this could lead to the buildup of a carbonaceous passivating layer preventing HF from removing the last few monolayers of oxide from the surface. This would be in agreement with the observed large amounts of non-carbidic carbon left on the surface after the HF dip. The observed similarities between SiC surfaces of different orientations supports this explanation, as well. Finally, it could be that some if not all of the oxygen is bonded to carbon instead of silicon. Indeed, the peak position of the non-carbidic C 1s peak XPS suggests that some carbon is bonded to oxygen at the surface. However, others have shown that by annealing in UHV at 700°C, this non-carbidic carbon desorbs from the surface still leaving behind ≈ a 1/2 monolayer of oxide on the surface [7,8]. The work of Mizokawa *et al.* [9] however, argues that even after thermal

desorption at 700°C significant amounts of oxygen are still bonded to carbon at the surface. In reality, a combination of all three explanations is probably responsible for the larger oxygen surface coverages observed for SiC surfaces after an HF dip.

$(0001)_{Si}$ 6H-SiC, As Polished. The results above show that $(0001)_{Si}$ 6H-SiC surfaces, which are not oxidized after polishing, as received are hydrophobic before and after dipping in 10:1 HF. In contrast to $(0001)_{Si}$ surfaces which have been oxidized, much smaller amounts of oxygen were found to be present on the surface before even an HF dip. This is somewhat consistent with the observation of hydrophobic and hydrophilic surfaces for these two surfaces. However, the most important difference observed between the oxidized and unoxidized surfaces, perhaps, is the identification of large amounts of fluorine on the unoxidized surface prior to an HF dip. One obvious source of this fluorine is the polishing procedure used by Cree. Unfortunately, this procedure is proprietary and we cannot comment. An alternative source of fluorine, however, could be the Fluoroware containers in which the SiC wafers were delivered. Most plastics contain additives to lower the glass transition temperature of the polymer and make a more ductile/less brittle plastic. These "plasticizers" are known to have high vapor pressures and outgas from the plastic. It is quite possible that fluorocarbon-based plasticizers have outgassed from the Fluoroware container and deposited on the unoxidized $(0001)_{Si}$ 6H-SiC surface. This would explain the third C 1s peak detected at 285.8 eV on these surfaces and could allow it to be assigned to C-F bonding. It would also explain the observation that like Teflon, this surface is essentially hydrophobic in all acid and bases except for extended exposure to acids and bases which are particularly aggressive at attacking organics and carbon contaminants.

The observation that an as received unoxidized/as polished $(0001)_{Si}$ 6H-SiC surface is converted from a hydrophobic to a hydrophilic surface on removal of a fluorine/fluorocarbon passivation layer indicates that this surface is not related to the well-known hydrophobic, hydrogen-terminated Si surface. The simple observation that the as polished $(0001)_{Si}$ 6H-SiC surface is hydrophobic in HNO_3 and Aqua Regia whereas hydrogen terminated Si (111) is not, bares this out.

Si Passivation Layer. As the source and exact nature of the fluorine/fluorocarbon passivation layer remains somewhat dubious to the authors, a more controllable passivation layer based on a 200Å Si capping layer was investigated. As demonstrated above, this capping layer behaves similarly in acids and bases to Si (111) surfaces and can be easily removed *in situ* by annealing in UHV at 1000-1100°C for 5-10 min. Hence, this allows one to more freely borrow from the wealth of knowledge developed in *ex situ* processing of silicon. The use of this capping layer was also found to result in lower outgassing rates in vacuum due to the production of a hydrophobic surface preventing HF from being trapped in micropipes. The authors would like to point out that the Si capping layer has an added advantage in that it can be

incorporated into existing processing routes. The Si capping layer could be deposited during cooling from SiC thin film CVD epitaxy. Rupp *et al.* [19], have currently demonstrated the ability to control the surface stoichiometry of SiC epitaxial films by controlling the gas phase composition in their LPCVD system during cooling. So, deposition of 20-200Å of Si during cooling after SiC epitaxial growth is certainly conceivable.

E. Conclusions

In conclusion, it has been found that: 1) removal of a thermal oxide from SiC surfaces using 10:1 HF leaves a hydrophilic surface, despite crystallographic orientation; 2) non-oxidized (0001)Si 6H-SiC surfaces as received are hydrophobic: a) a fluorine/fluorocarbon termination is associated with the hydrophobic nature of this surface and b) removal of the fluorine termination leaves a hydrophilic surface; and 3) a 200Å Si capping layer provides a hydrophobic passivating layer which can be removed *in situ* via thermal desorption at 1100°C.

F. References

1. W. Kern, J. Electrochem. Soc. **137** (6), 1887 (1990).
2. G. R. Srinivasan and B. S. Meyerson, J. Electrochem. Soc. **134** (6), 1518 (1987).
3. B. S. Meyerson, E. Ganin, D. A. Smith, and T. N. Nguyen, J. Electrochem. Soc. **133** (6), 1232 (1986).
4. M. K. Sanganeria, M. C. Ozturk, G. Harris, K. E. Violette, I. Ban, C. A. Lee, and D. M Maher, J. Electrochem. Soc. **142** (11), 3961 (1995).
5. R. Williams, *Modern GaAs Processing Methods*, 2nd ed. (Artech House, Inc., New York, 1990), pp. 81-114.
6. F. K. LeGoues, MRS Bulletin **21**, 38 (1996).
7. L. M. Porter, R. F. Davis, J. S. Bow, M. J. Kim, R. W. Carpenter, R. C. Glass, J. Mater. Res. **10** (3), 668 (1995).
8. H. Tsuchida, I. Kamata, and K. Izumi, Jpn. J. Appl. Phys. **34**, 6003 (1995).
9. Y. Mizokawa, S. Nakanishi, O. Komoda, S. Miyase, H. S. Diang, C. Wang, N. Li, and C. Jiang, J. Appl. Phys. **67** (1), 264 (1990).
10. U. Starke, Ch. Bram, P.R. Steiner, W. Hartner, L. Hammer, K. Heinz, K. Muller, Appl. Surf. Sci. **89**, 175 (1995).
11. M. E. Lin, S. Strite, A. Agarwal, A. Salvador, G. L. Zhou, M. Teraguchi, A. Rockett, and H. Morkoc, Appl. Phys. Lett. **62**, 702 (1993).
12. B. S. Meyerson, F. J. Himpsel, and K. J. Uram, Appl. Phys. Lett. **57**, 1034 (1990).
13. M. Grundner and H. Jacob, Appl. Phys. A **39**, 73 (1986).
14. Y. J. Chabal, G. S. Higashi, K. Raghavachari, and V. A. Burrows, J. Vac. Sci. Technol. A **7** (3), 2104 (1989).
15. G. S. Higashi, R. S. Becker, Y. J. Chabal, A. J. Becker, Appl. Phys. Lett. **58**, 1656 (1991).
16. G. S. Higashi, Y. J. Chabal, G. W. Trucks, and K. Raghavachari, Appl. Phys. Lett. **56**, 656 (1990).
17. M. Houston and R. Maboudian, J. Appl. Phys. **68**, 3801 (1995).
18. R. Rupp, Presentation on Spring 1996 MRS Meeting.

IV. Rectifying and Ohmic Contacts for P-type Alpha (6H) Silicon Carbide

A. Introduction

The formation of low resistivity and thermally stable ohmic contacts to 6H-SiC remains a serious problem in the development of SiC device technology. For SiC power devices to have the advantage over Si, the contact resistivities must be below 1×10^{-5} Ω-cm^2 [1]. The thermal stability of ohmic contacts is of particular concern for p-type SiC, which have traditionally contained Al to dope the SiC surface below the contacts. While the fabrication of ohmic contacts to SiC also has usually depended on very heavily-doped surfaces, the large barrier heights associated with metals on p-type SiC limit the achievable contact resistivities. Based on all of these issues and experiments already performed at NCSU, our goals are to produce contacts which are thermally stable, oxidation resistant and have low contact resistivities.

Low resistance contacts to p-type SiC remain a substantial challenge for high temperature and high-power devices. An Al-Ti alloy [2] annealed at 1000°C for 5 min. was reported to yield contact resistances ranging from 2.9×10^{-2} Ω cm^2 for a carrier concentration of 5×10^{15} cm^{-3} to 1.5×10^{-5} Ω cm^2 for 2×10^{19} cm^{-3}. The thermal stability of these contacts was not reported. Aluminum deposited on a heavily-doped 3C-SiC interlayer on a 6H-SiC substrate and subsequently annealed at 950°C for 2 min. reportedly yielded contact resistivities of $2\text{–}3\times10^{-5}$ Ω cm^2 [3]. Because of its low melting point (660°C), however, pure Al would be unsuitable for high temperature applications. Platinum contacts annealed from 450 to 750°C in 100°C increments were also used as ohmic contacts to p-type SiC [4]. These contacts, which rely on the combination of a highly-doped surface and the high work function of Pt, have not been known to yield contact resistivities as low as those for contacts containing Al.

This report compares the electrical and chemical characterization of annealed Al-based (NiAl) and B-based (Cr-B) contacts on p-type 6H-SiC. In particular, the current-voltage characteristics and oxidation properties were investigated before and after annealing at 1000 °C. In addition, the electrical properties of Schottky contacts on p-type SiC were measured and compared to typical behavior found previously for Schottky contacts on n-type SiC.

B. Experimental Procedure

Vicinal, single-crystal 6H-SiC (0001) wafers provided by Cree Research, Inc. were used as substrates in the present research. The wafers were doped with N or Al during growth to create n- or p-type material, respectively, with carrier concentrations of $1\text{–}5\times10^{18}$ cm^{-3}. Homoepitaxial layers (1–5 μm thick) grown by chemical vapor deposition (CVD) were Al-doped with carrier concentrations ranging from 1×10^{16} to 1×10^{19} cm^{-3}. The surfaces were oxidized to a thickness of 500–1000 Å in dry oxygen. The substrates were cleaned using a 10

min. dip in 10% hydrofluoric acid, transferred into the vacuum system, and heated at 700°C for 15 min. to remove any residual hydrocarbon contamination.

A UHV electron beam evaporation system was used to deposit the NiAl, Ni, Au, Pt, and Cr-B films. After depositing 1000 Å of NiAl, 500–1000 Å of Ni was deposited as a passivating layer. Pure Ni (99.99%) and pure Al (99.999%) pellets were arc melted to form alloyed pellets of 50:50 atomic concentration for evaporation of NiAl. The films were deposited onto unheated substrates at a rate of 10–20 Å/s. Chromium and B were evaporated simultaneously from separate evaporation sources. The pressure during the depositions was between 5×10^{-9} and 5×10^{-8} Torr.

Circular contacts of 500 μm diameter were fabricated for electrical characterization by depositing the metal films through a Mo mask in contact with the substrate. Silver paste served as the large area back contact. For contact resistance measurements, TLM patterns [5] were fabricated by photolithography. The Ni/NiAl films were etched in phosphoric acid : acetic acid : nitric acid (12 : 2 : 3) at 50°C (etch rate ≈ 30 Å/s). The contact pads were 300×60 μm with spacings of 5, 10, 20, 30 and 50 μm. Mesas in the substrate were not fabricated. All annealing was conducted in a N_2 ambient in a rapid annealing furnace.

Electrical characteristics were obtained from current-voltage and capacitance-voltage measurements. Current-voltage (I-V) measurements were obtained with a Rucker & Kolls Model 260 probe station in tandem with an HP 4145A Semiconductor Parameter Analyzer. Capacitance-voltage (C-V) measurements were taken with a Keithley 590 CV Analyzer using a measurement frequency of 1 MHz.

Auger electron spectroscopy (AES) was performed with a JEOL JAMP-30 scanning Auger microprobe. The films were sputtered with Ar ions at a beam current and voltage of 0.3 μA and 3 kV, respectively, to obtain composition profiles through the thickness of the films.

C. Results and Discussion

Chemical Characterization of As-deposited Films. An Auger depth profile of a film deposited from the NiAl source showed that the overall composition remained relatively stable. The relative compositions of Ni and Al were calculated by referencing to pure Ni and pure Al standards and accounting for their corresponding sensitivity factors. The average atomic composition was approximately 50:50. With reference to Cr and B standards, the first Cr-B film co-deposited by e-beam evaporation was determined to be comprised of approximately 20% Cr and 80% B (CrB_4). While a thin oxide layer was detected at the surface of the NiAl film, no O was detected within either of the films. After recalibrating the thickness monitors for Cr and B, films were deposited with an intended composition of CrB_2.

Schottky Contacts. In the as-deposited condition the Ni/NiAl contacts were rectifying on p-type SiC with carrier concentrations of 1.6×10^{16} and 3.8×10^{18} cm^{-3} in the epilayer. The

sample with the lower carrier concentration displayed leakage current densities of ~1×10^{-8} A/cm^2 at 10 V and ideality factors between 1.4 and 2.4, while the latter sample displayed approximately five orders of magnitude higher leakage current densities and similar ideality factors. The average Schottky barrier heights (SBH's) calculated for the samples with the lower and higher carrier concentrations were 1.37 and 1.26 eV, respectively. The lower SBH calculated for the former sample is likely due to enhanced thermionic field emission through the upper energy region of the barrier because of the narrower depletion region. Hence, the 1.37 eV value is believed to be more accurate.

Similar results were obtained for as-deposited Ni, Au, and Pt contacts on p-type (2.1–4.5$\times10^{16}$ cm^{-3}) 6H-SiC (0001). These samples displayed similar leakage currents and ideality factors of 1.3–2.1 and <1.1, respectively. From these measurements SBH's of 1.31 eV for the Ni contacts and 1.27 eV for the Au contacts were calculated. In comparison, as-deposited Ni on n-type (4.1×10^{16} cm^{-3}) 6H-SiC (0001) yielded ideality factors below 1.1, similar leakage current densities to those stated above, and SBH's of 1.14 eV and 1.21 eV calculated from I-V and C-V measurements, respectively.

Our measurements on p-type SiC have shown consistent differences from measurements on n-type 6H-SiC. The SBH's tended to be higher on p-type than on n-type material. While leakage currents for Au, NiAl, and Ni contacts on p-type 6H-SiC were comparable to Ni contacts on n-type 6H-SiC, the ideality factors were higher on p-type SiC. These ideality factors and SBH's are higher than for Ni contacts (and other previously studied contacts) on n-type 6H-SiC (0001). The higher ideality factors indicates that thermionic emission was not the dominant current transport mechanism in the p-type SiC and may indicate the occurrence of recombination at deep levels.

Conversely, the relationship between the SBH's of the metals on p-type SiC and their respective work functions was similar to that which we previously found for n-type SiC. The calculated SBH's on p-type SiC are plotted vs. the metal work functions in Fig. 1. The work function for NiAl was taken to be the average of the work functions for pure Ni and pure Al since a value was not found in the literature for NiAl. The slope of the line fit to the empirical data was -0.28 as compared to a slope of -1.0 for the theoretical data. These results indicate that surface states on p-type 6H-SiC (0001) cause a partial pinning of the Fermi level, in agreement with the results of our previous, extensive study on n-type SiC.

Ohmic Contacts. The Ni/NiAl contacts were sequentially annealed for total times of 10–80 s at 1000 °C in a N_2 ambient. This temperature was used because (1) limited intermixing of Al and SiC was reported at 900°C [6] and (2) other papers report annealing in this temperature range for Al-based ohmic contacts on p-type SiC [2,3,7]. Because of the extremely high thermodynamic driving force for Al to form an insulating oxide layer (ΔG_f (Al_2O_3) ~ -1300 kJ/mol at 1000 °C [JANAF - Chase, M., et al., JANAF Thermochem. Tables, 3d Ed. J. Phys.

Chem. Ref. Data, 1985. 14(Supp. 1)]), 1000 Å of Ni was deposited on top of the NiAl contacts to slow the oxidation process.

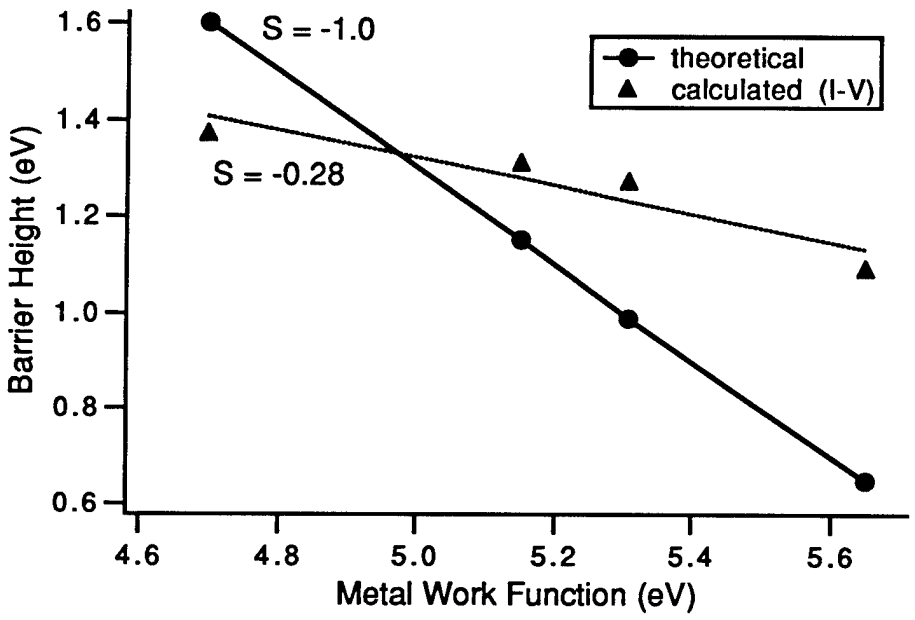

Figure 1. Graph of calculated and theoretical barrier heights of as-deposited NiAl, Au, Ni, and Pt contacts on p-type 6H-SiC vs. metal work function. The calculated values were determined from I-V measurements, and the theoretical values were calculated according to the Schottky-Mott limit. The slopes, S, of the lines fit to each set of data are indicated on the graph.

The calculated specific contact resistivities of Ni/NiAl on p-type SiC (1.5×10^{19} cm^{-3} in the epilayer) after annealing at 1000°C (Ar ambient) for 20, 40, 60, and 80 s were 2.0×10^{-2}, 1.9×10^{-2}, 2.2×10^{-2}, and 3.1×10^{-2} Ω cm^2, respectively. The additional force on the probes needed to obtain consistent results indicates that an oxide began to form at the surface which would likely cause more severe problems if the samples were annealed further. The increase in contact resistivity is believed to be due to the surface oxide layer.

An Auger depth profile (Fig. 2) of Ni/NiAl/SiC annealed at 1000°C for 80 s in Ar shows that a surface oxide formed during the annealing process. After sputtering for a couple of minutes, the O concentration dropped to below detectable limits; however, the data shows a decreasing Al concentration in the direction toward the SiC interface. This indicates that the kinetics are more favorable for the Al to diffuse toward the surface and react with O than for the Al to react with the SiC. Some of the Ni has probably reacted with Si at the interface to form a silicide, as indicated by the local maximum in the Ni intensity near the SiC interface, while the peak in the C intensity indicates the presence of an adjacent C-rich layer.

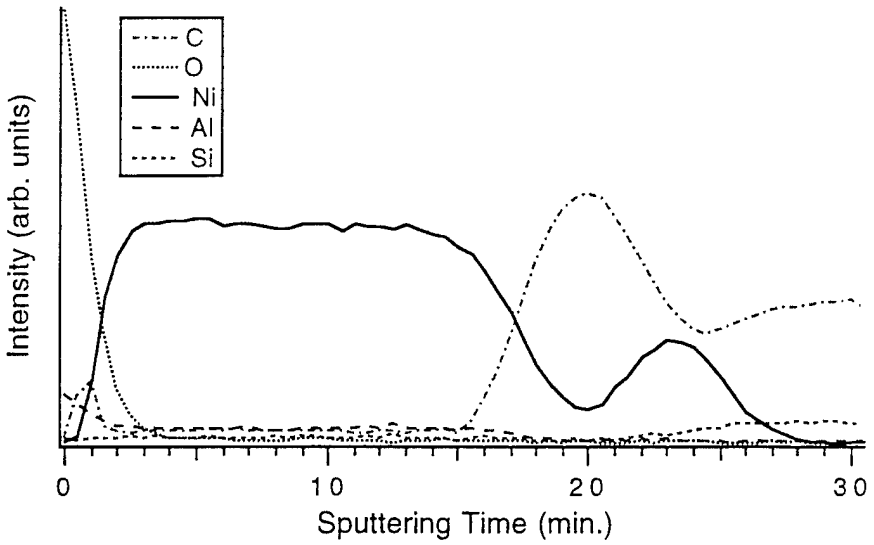

Figure 2. AES composition profile of Ni (1000 Å) / NiAl (1000 Å) / 6H-SiC annealed at 1000 °C for 80 s in N_2.

The demonstrated oxidation problem with Al necessitates the development of ohmic contacts which do not consist of substantial concentrations of Al. To reduce this problem we have chosen to investigate contacts which contain B.

The main reasons for choosing B are that it is also a p-type dopant in SiC, its oxide is not as stable, and it is a much faster diffusant in SiC. Table I compares some important properties of B, Al, and their associated oxides. Recent reports [8-10] show that the 'shallow' activation energy for B in SiC is significantly less than previously reported. Boron compounds tend to be more stable at high temperatures than aluminum compounds which suffer from the low melting point of Al. Also, the diffusion coefficient of B is at least three orders of magnitude greater than that of Al. Therefore, more B than Al will diffuse into the SiC at lower temperatures. As discussed, a major problem with Al-based contacts is the strong driving force for forming an insulating oxide layer. This situation is shown by the extremely low equilibrium partial pressure, p_{O2}, for Al_2O_3 formation. While B_2O_3 also has a low p_{O2}, it is significantly higher

Table I. Selected Properties of B, Al, and Associated Oxides

Element	Activation Energy in 6H-SiC (meV)	Solid Source Diffusion, DSiC @ 1800°C (cm2/s)	Equilibrium Partial Pressure of O_2, pO_2 @ 700°C (Torr)	Melting Temp. of the associated oxide, T_{melt} (°C)
B	300 [8-10]	10^{-11} [11-12]	10^{-35}	450
Al	200 [9]	$<10^{-14}$ [13]	10^{-47}	2040

than that for Al_2O_3, indicating that the driving force for B to form an oxide is significantly lower. There is also a larger number of metals which would reduce the oxide formed with B than that formed with Al, a fact which is encouraging when one is trying to diffuse free B into SiC. Another advantage is that the melting point of boron oxide is notably low.

Several boron compounds which possess reasonably low resistivities and high melting temperatures are listed in Table II. We have chosen to investigate Cr-B contacts because of the relative ease to deposit these materials by electron beam evaporation and the demonstrated use of Cr in metallization schemes for diffusion barriers. The refractory nature of these materials increases the probability of forming ohmic contacts which will be stable at high temperatures.

Table II. Resistivities and Melting Points of Selected Boron Compounds

Material	Electrical Resistivity (μΩ cm) @ 298 K [14]	Melting Temp. (°C) [15]
B	$18x10^{11}$	2092
CrB2	30	2200
GdB4	31	2650
MoB	45	2600
NbB2	26	3000
TaB2	33	3037
VB2	23	2747
ZrB2	10	2972

Cr and B were simultaneously deposited on p-type 6H-SiC epitaxial layers, some of which had not been oxidized to prevent the reduction of the Al dopant near the surface during oxidation. The carrier concentrations in the epitaxial layers ranged from 1×10^{18} to 8×10^{18} cm^{-3}. The as-deposited contacts for the sample with a carrier concentration of 1×10^{18} cm^{-3} displayed rectifying behavior with low leakage currents (~4×10^{-8} at 10 V) and ideality factors between 1.5 and 1.9. Rectification was expected since the contacts had not been annealed, and large SBH's normally exist for as-deposited contacts on p-type SiC.

The samples were annealed at 1000°C for total times varying from 60 to 240 s in an Ar ambient. After 60 s at 1000°C, the contacts showed substantial changes in their electrical characteristics. With an increase in annealing time to 240 s, the contacts became more ohmic-like. An example of the I-V characteristics obtained after annealing at 1000°C for 240 s is shown in Fig. 3. However, after annealing for 300 s, the contacts became rectifying with high leakage currents; this result may be due to the formation of B_4C at the interface.

Although true ohmic behavior of Cr-B contacts has not yet been achieved, the improved oxidation resistance over that of the NiAl contacts in combination with the tendency toward ohmicity displayed in nonimplanted samples annealed at 1000 °C for 60–240 s makes the former contacts a potentially beneficial alternative to Al-based metallization. Higher surface carrier concentrations in the SiC epilayers and ion implantation of Al or B should improve the ohmic behavior of the contacts. Figure 4 shows an AES depth profile of Cr-B/SiC annealed at 1000°C for 360 s in Ar. The O signal diminished to below detectable limits after sputtering for approximately 10 s. The finite O level indicated in the profile is attributed to the tailing of the Cr peak due to overlapping energy windows for measuring the two peaks. No O peak was observed after sputtering into the film.

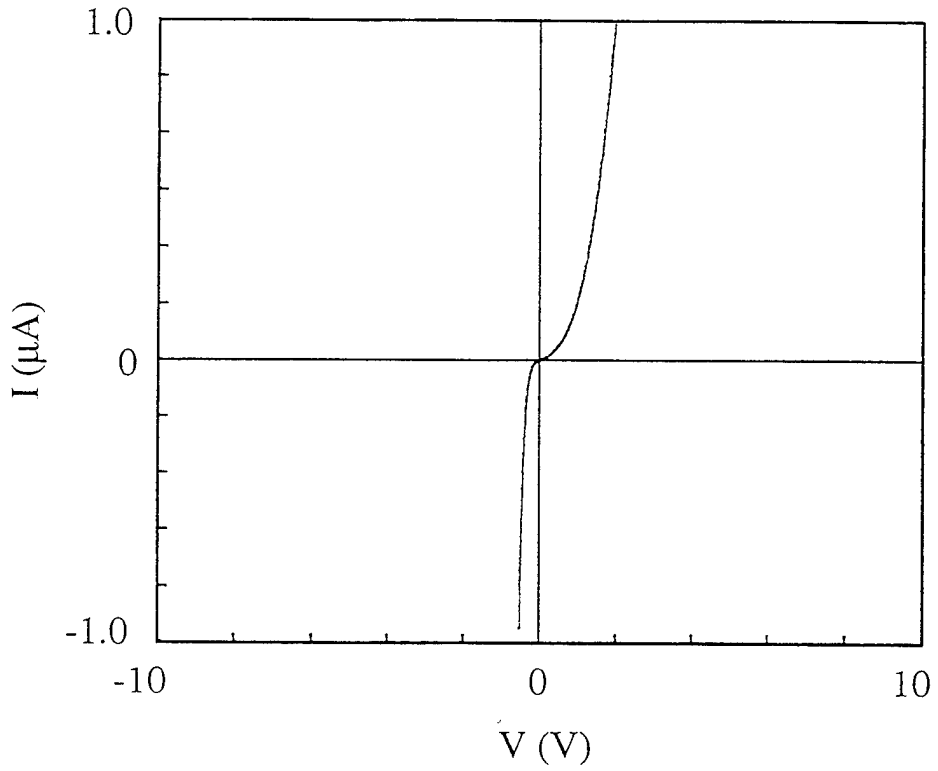

Figure 3. Current-voltage (I-V) characteristics of Cr-B on p-type 6H-SiC annealed at 1000 °C for 240 s in Ar.

D. Conclusions

Nickel-aluminum was investigated primarily as an ohmic contact for p-type 6H-SiC because of the p-type doping of Al in SiC, the high melting point of NiAl (as compared to Al), and the tendency of Ni to form silicides but not carbides. This latter property potentially could have resulted in extraction of Si from the SiC lattice in exchange for Al, thereby enhancing the p-type carrier concentration at the surface. Although the I-V measurements indicate that some

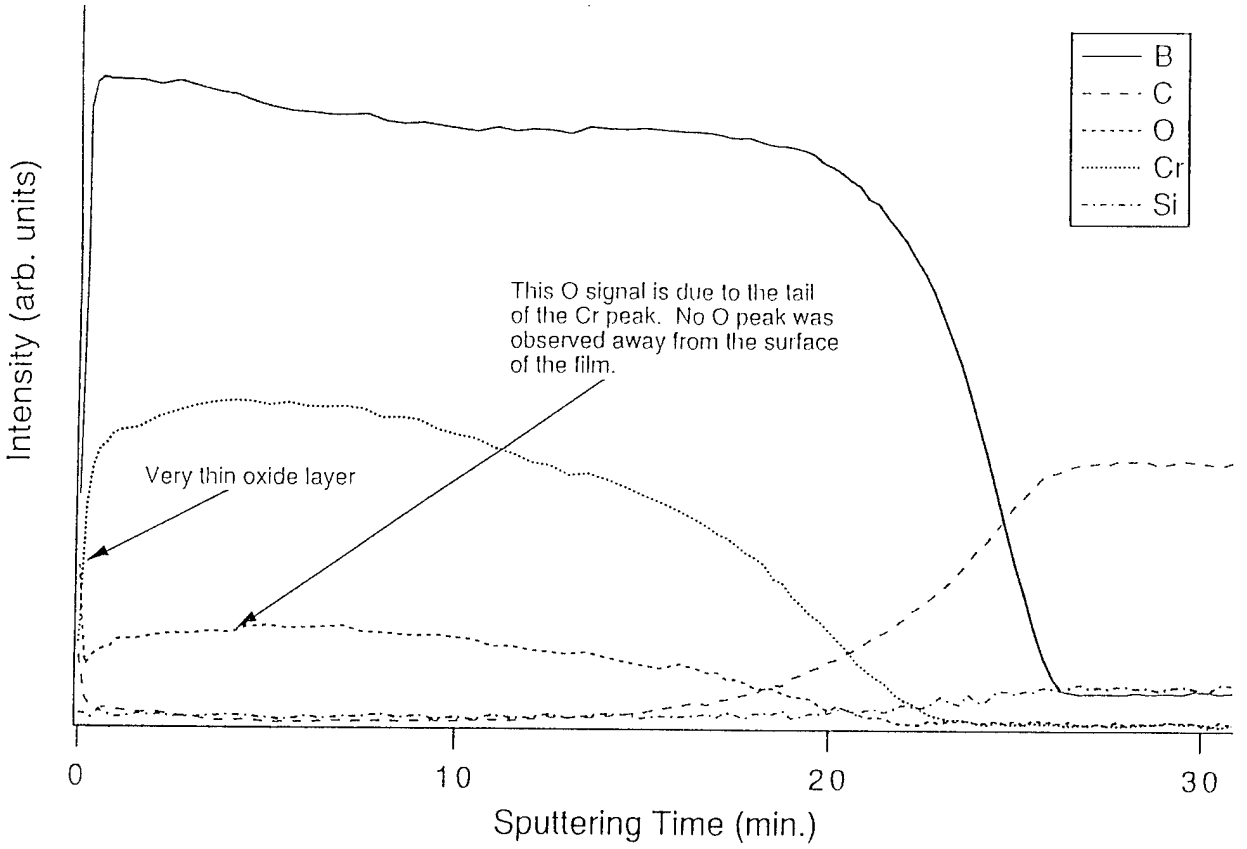

Figure 4. AES composition profile of Cr-B / 6H-SiC annealed at 1000 °C for 300 s and 1100 °C for 360 s in Ar.

Al may be diffusing into the SiC after the longest annealing time performed (80 s at 1000°C), this potential for reaction between Al and SiC appears to be exceeded by the driving force for Al to diffuse to the surface and react with O. A concentration profile obtained from AES analysis shows that Al has diffused through the 1000 Å Ni overlayer to form a thin (200 Å estimated) oxide layer.

In addition to the ohmic behavior resulting from annealing the NiAl contacts, as-deposited Ni, NiAl, and Au contacts deposited at room temperature on p-type ($N_A < 5\times10^{16}$ cm^{-3}) 6H-SiC (0001) were rectifying with low leakage currents, ideality factors between 1.3 and 2.4, and SBH's of 1.31, 1.27, and 1.37 eV, respectively. These results indicate that the Fermi level is partially pinned at p-type SiC surface, in agreement with our previous results on n-type SiC.

As an alternative to Al for fabricating ohmic contacts to p-type 6H-SiC, Cr-B was investigated because of its low resistivity, high melting temperature, high diffusivity of B in SiC, and reduced tendency for oxidation (compared to that of Al). In the as-deposited condition these contacts were rectifying with low leakage currents. After annealing at 1000 °C for 60 s, the contacts displayed semi-ohmic behavior and became less resistive with successive 60 s

anneals to a total time of 240 s. The contacts showed rectification after annealing for 300 s, a result which may be associated with the formation of B_4C at the interface. The most promising result was the substantially improved oxidation resistance.

E. Future Research Plans and Goals

Electrical characterization of the Cr-B contacts as a function of annealing time and surface carrier concentration (both *in situ* doping and ion implantation) will be continued. Contact resistivities will be calculated from transmission line model (TLM) measurements to optimize the processing conditions. Transmission electron microscopy will be performed to identify phases formed at the interfaces and to use as feedback for the optimization.

F. References

1. D. Alok, B. J. Baliga, and P. K. McLarty, IEDM Technical Digest **IEDM 1993**, 691 (1993).
2. J. Crofton, P. A. Barnes, J. R. Williams, and J. A. Edmond, Appl. Phys. Lett. **62** (4), 384 (1993).
3. V. A. Dmitriev, K. Irvine, and M. Spencer, Appl. Phys. Lett. **64** (3), 318 (1994).
4. R. C. Glass, J. W. Palmour, R. F. Davis, and L. S. Porter, U.S. Patent No. 5,323,022 (1994).
5. H. H. Berger, Solid State Electron. **15** (2), 145 (1972).
6. V. M. Bermudez, J. Appl. Phys. **63** (10), 4951 (1988).
7. T. Nakata, K. Koga, Y. Matsushita, Y. Ueda, and T. Niina, in *Amorphous and Crystalline Silicon Carbide and Related Materials II*, M. M. Rahman, C. Y.-W. Yang, and G. L. Harris (eds.), Vol. 43, (Springer-Verlag, Berlin, 1989).
8. W. Suttrop, G. Pensl, and P. Lanig, Appl. Phys. Lett. **A 51**, 231 (1990).
9. W. C. Mitchel, M. Rogh, A. O. Evwaraye, P. W. Yu, and S. R. Smith, J. Electronic Mater. **25** (5), 863 (1996).
10. E. N. Mokhov, Y. A. Vodakov, G. A. Lomakina, V. G. Oding, G. F. Kholuanov, and V. V. Semenov, Soviet Physics - Semiconductors **6** (3), 414 (1972).
11. G. Pensl and W. J. Choyke, Phys. B **185**, 264 (1993).
12. E. N. Mokhov, Y. A. Vodakov, and G. A. Lomakina, Soviet Physics - Solid State **11** (2), 415 (1969).
13. C. van Opdorp, Solid State Electronics **14**, 613 (1971).
14. G. V. Samsonov and I. M. Vinitskii, *Handbook of Refractory Borides* (Plenum Press, New York, 1980).

V. Characterization of Oxides on N- and P-type 4H- and 6H-SiC

A. Introduction

Silicon carbide (SiC) has been shown to be an excellent material for the fabrication of devices for high-power, high-frequency and high-temperature applications [1]. The advantages of SiC metal oxide semiconductor field effect transistors (MOSFETs) has also been discussed [2]. The successful operation of these devices hinges on the interface and bulk properties of the gate dielectric, usually an oxide. Previous researchers have reported results on thermally grown oxides on N-type [3-6] and P-type 6H-SiC [5,7-11]. While the results obtained on N-type 6H-SiC have shown that those oxides are of high quality, oxides grown on P-type 6H-SiC exhibit large flatband voltage shifts and are thus unsatisfactory for application as gate dielectrics. Oxides deposited under special conditions with surface preparation specific to the particular deposition might show improved interfacial properties over thermally-grown oxides.

The SiO_2-SiC interfaces will be characterized using capacitance-voltage (C-V) measurements [12]. A mask set has been designed to fabricate the MOS structures required for accurate and complete electrical characterization. Device processing was commenced and completed during the last quarter. C-V measurements were performed on the MOS capacitors and MOS-gated diodes during the present quarter.

B. Experimental Procedure

In the proposed process, the wafer would first be subjected to a sacrificial oxidation to clean the surface. This sacrificial wet oxidation was performed both on the 6H-SiC and 4H-SiC wafer, as well as a monitor 6H-SiC wafer. The wafers were first subjected to an RCA clean (5 minutes in $NH_4OH:H_2O_2:H_2O$::1:1:5 at 75°C followed by a 5 minute rinse followed by 5 minutes in $HCl:H_2O_2:H_2O$::1:1:5 at 75°C followed by a 5 minute rinse) with no subsequent BOE dip. The wafers were then subjected to dry-wet-dry oxidation for 5-240-5 minutes at 1100°C. The resultant oxide thicknesses were ellipsometrically measured using a Gaertner ellipsometer. The 6H-SiC wafer had a mean oxide thickness of 266A with a standard deviation of 3.3A and the 4H-SiC wafer had a mean oxide thickness of 311A with a standard deviation of 4.4A. The mean oxide thickness on the monitor 6H-SiC wafer was 267A with a standard deviation of 8.1A.

A low temperature oxide (LTO) of thickness 7000A was then deposited on the wafer. This LTO acts as a mask for the subsequent implant step. Subsequent to patterning this layer of LTO, a further 1000A of LTO was deposited to act as a pad oxide during the source implant to keep the maximum dopant concentration at the surface and not inside the semiconductor. A two step N^+ implant was performed at MCNC (dose=2×10^{15} cm^{-2}:energy=80keV::dose= 1×10^{15} cm^{-2}: energy=40keV). While the mean thickness of the first LTO layer can have some

variability since its only function is to act as an implant mask, the mean thickness of the second LTO layer must be very close to 1000A as the doses and energies of the subsequent implant steps have been designed and optimized taking into account a pad oxide thickness of 1000A.

The wafer was then subjected to a high temperature anneal at 1250°C for 30 minutes in argon + 1% oxygen to activate the dopant. The 1% oxygen is included to prevent the evaporation of Si during the argon anneal. The LTO was then further patterned to define the gate region and the gate dielectric thermally grown on the SiC. The thermal oxidation conducted in pyrogenic steam at 1100°C for 240 minutes with a 5 minute dry oxidation preceding it. The oxidation temperature was then reduced to 900°C and further wet oxidation was performed for 30 minutes. A final 5 minute dry oxidation step was performed before ramping down in N_2 to the furnace idling temperature of 750°C.

A blanket deposition of silicon was then done after performing an RCA clean on the wafers. The thickness of the silicon, which was amorphous was measured using Nanometrics and found to be 4200A with a variation of 5%. The wafers were cleaned again with a RCA clean and heavily doped N^+ with phosphorus disks at 900°C for 30 minutes. This converted the amorphous silicon into polysilicon. The sheet resistivity of the poly was measured using a 4 point probe to be around 31 Ω/o. This is satisfactorily low.

The poly was then patterned using reactive ion etching (RIE) using a SF_6/O_2 gas mix. The backside of the wafer was also subjected to a blanket RIE to remove the poly deposited thereon. The resist layer used to define the poly patterning was removed using a oxygen plasma. Negative resist was then spun on the wafer and patterned so that the metal regions could be obtained by lift-off. Prior to loading in the evaporator, the wafers were etching in a very dilute HF solution to remove any native oxides or oxide remaining on the regions to receive the metal. Sequential evaporation of Ti followed by Al was done on the frontside of the wafers. A blanket evaporation of Al was done on the backside of the wafers to provide an ohmic contact. The frontside metal was then subjected to lift-off to define the metal regions. The wafers were then subjected to a forming gas anneal at 450°C for 15 minutes.

C. Measurements

C-V measurements were performed on MOS capacitors and MOS-gated diodes on 4H- and 6H-SiC. Measurements performed on MOS capacitors showed typically high flatband voltage shifts corresponding to effective oxide charges of 2×10^{12} cm^{-2}. The measured C-V curves are shown in Fig. 1 and Fig. 2. C-V measurements performed on MOS-gated diodes showed some interesting "hook and ledge" features. An average interface state density could be estimated from these curves to be $6.4\times10^{11}cm^{-2}\,eV^{-1}$. Similar characteristics had been reported by Goetzberger [13] for MOS gated diodes on silicon at 77K. He states that similar results are to be expected for wide band gap semiconductors at room temperature and that is indeed

observed in SiC as shown in Fig. 3. It is strongly emphasized that typical simultaneous hi-lo C-V measurements at room temperature on MOS-capacitors will *not* yield accurate D_{it} information more than a few 100 meV away from the valence band. While the MOS gated diode yields only an average D_{it}, it does so over a range of 2.5eV from close to accumulation to inversion.

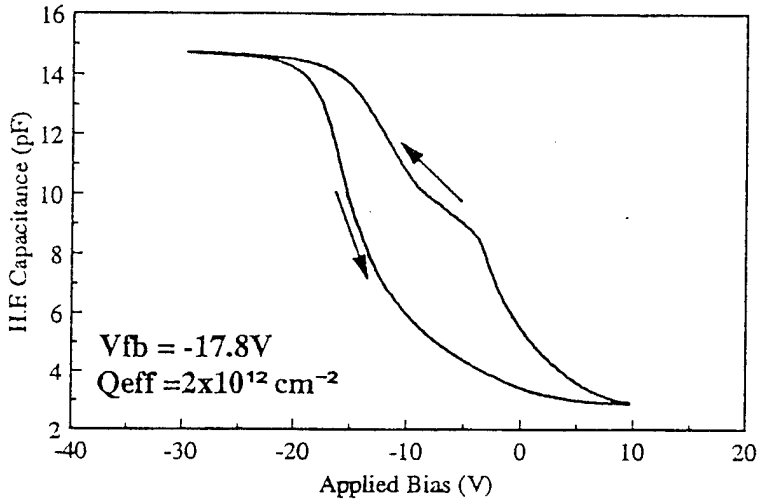

Figure 1. C-V curves on MOS capacitors on 6H-SiC.

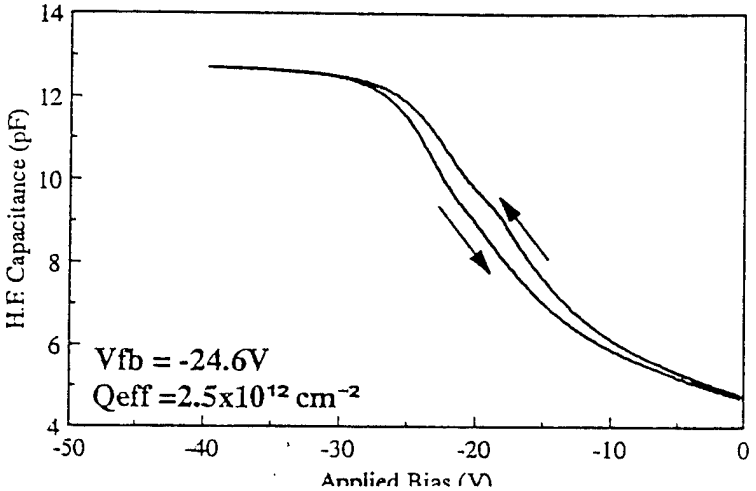

Figure 2. C-V curves on MOS capacitors on 4H-SiC.

D. Conclusions

The fabrication of the MOS capacitors and MOS gated diodes was completed during this quarter and C-V measurements made on these devices. An effective charge density of about 2.2×10^{12} cm^{-2} and an average interface trap density of 6.4×10^{11} $cm^{-2}eV^{-1}$ were measured on these films.

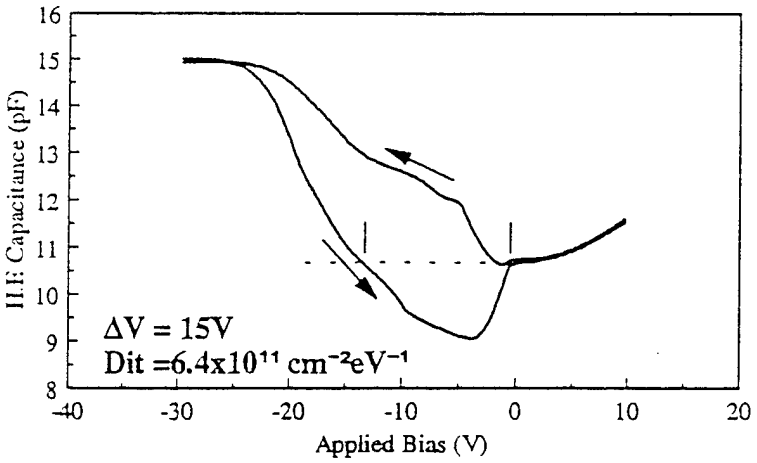

Figure 3. C-V curves on MOS gated diodes on 6H-SiC.

E. Future Research Plans and Goals

Characterization of deposited oxide films will begin as soon as possible.

F. References

1. R. J.Trew, J-B. Yan, and P. M.Mock, Proc. IEEE **79**, 598 (1991).
2. M. Bhatnagar and B. J.Baliga, IEEE Trans. on Electron Devices **40**, 645 (1993).
3. A. Suzuki, H. Ashida, N. Furui, K. Mameno and H. Matsunami, Jpn. J. of Applied Physics **21**, 579 (1982).
4. D. Alok, P. K. McLarty, and B. J. Baliga, Applied Phys. Lett. **64**, 2845 (1994).
5. T. Ouisse, N. Becourt, C. Jaussaud, and F. Templier, J. of Applied Physics **75**, 604, (1994).
6. P. Neudeck, S. Kang, J. Petit, and M. Tabib-Azar, J. of Applied Physics **75**, 7949 (1994).
7. C. Raynaud, J-L. Autran, B. Balland, G. Guillot, C. Jaussaud and T. Billon, J. of Applied Physics **76**, 993 (1994).
8. D. Alok, P. K. McLarty, and B. J. Baliga, Applied Phys. Lett. **65**, 2177 (1994).
9. J. N. Shenoy, G. L. Chindalore, M. R. Melloch, J. A. Cooper Jr., J. W. Palmour and K. G.I rvine, Journal of Electronic Materials **24**, 303 (1995).
10. J. N. Shenoy, L. A. Lipkin, G. L. Chindalore, J. Pan, J. A. Cooper Jr., J. W. Palmour and M. R. Melloch, Proc. 21st Intl. Symp. on Compound Semiconductors, 499, San Diego (1994).
11. S. T. Sheppard, M. R. Melloch and J. A. Cooper Jr., IEEE Trans. on Electron Devices **41**, 1257 (1994).
12. E. H. Nicollian and J. R. Brews, MOS Physics and Technology, Wiley (1991).
13. A. Goetzberger and J. C. Irvin, IEEE Trans. on Electron Devices **15**, 1009 (1968).

VI. Distribution List

Mr. Max Yoder Office of Naval Research Electronics Division, Code: 312 Ballston Tower One 800 N. Quincy Street Arlington, VA 22217-5660	3
Administrative Contracting Officer Office of Naval Research Regional Office Atlanta 101 Marietta Tower, Suite 2805 101 Marietta Street Atlanta, GA 30323-0008	1
Director, Naval Research Laboratory ATTN: Code 2627 Washington, DC 20375	1
Defense Technical Information Center 8725 John J. Kingman Road Suite 0944 Ft. Belvoir, VA 22060-6218	2